Taylor & Francis
Taylor & Francis Group

On helical multiscale characterization of homogeneous turbulence

Frank G. Jacobitz[a], Kai Schneider[b], Wouter J.T. Bos[c], and Marie Farge[d]

[a] *Mechanical Engineering Program, University of San Diego, San Diego, California, USA;*
[b] *M2P2-CNRS & CMI, Aix-Marseille Université, Marseille Cedex 13, France;* [c] *LMFA-CNRS, Ecole Centrale de Lyon, Université de Lyon, Ecully Cedex, France;* [d] *LMD-IPSL-CNRS, Ecole Normale Supérieure, Paris Cedex 5, France*

The helical properties of five prototypical homogeneous turbulent flows are investigated: statistically steady forced isotropic turbulence, decaying isotropic turbulence, decaying rotating turbulence, growing sheared turbulence, and growing rotating sheared turbulence with a rotation ratio $f/S = +0.5$. The five turbulent flows were originally studied using direct numerical simulations, and well-developed flow fields are chosen for this analysis. For comparison, a solenoidal uncorrelated Gaussian random field is included in the analysis as a sixth case. An orthogonal wavelet decomposition is used to study the scale-dependent properties of the cases. It is found that flows with growing turbulent kinetic energy and turbulent motion at large scales show a maximum in the relative kinetic helicity probability distribution functions (PDFs) at zero, corresponding to a trend to local two-dimensionalization of the flow with vorticity and velocity tending to be perpendicular. Flows with decaying turbulent kinetic energy and turbulent motion at small scales, however, show maxima of the relative kinetic helicity PDFs at plus and minus one, indicating a preference for helical motion with a trend to alignment or anti-alignment of vorticity and velocity. The PDFs of relative super-helicity always assume maxima at plus and minus one for all flows. The helical properties of statistically steady forced isotropic turbulence follow those of flows with decaying turbulent kinetic energy and a small asymmetry in the relative helicity PDFs is observed. Joint PDFs of relative kinetic helicity and relative super-helicity show that the quantities tend to have the same sign for all flows, including the random field, indicating that super-helicity dissipates kinetic helicity.

Keywords: helicity; homogeneous isotropic and anisotropic turbulence; scale-dependent statistics; direct numerical simulation

1. Introduction

The helicity of a solenoidal vector field is a scalar valued signed quantity defined by the scalar product of a vector with the inverse of its curl, i.e., the Biot–Savart integral. For example, the kinetic helicity is defined as $H_u = \boldsymbol{u} \cdot \boldsymbol{\omega}$, where $\boldsymbol{u}$ is the velocity and $\boldsymbol{\omega} = \nabla \times \boldsymbol{u}$ is the vorticity. The mean kinetic helicity, defined as $\langle H_u \rangle = \int H_u d^3 x$, was introduced to study turbulence [1]. It was shown to provide a measure for the linkage of vortex lines and it is conserved in the inviscid limit of the Navier–Stokes equations [2–4]. Furthermore, helicity allows to quantify the effects that are due to a lack of reflectional symmetry or chirality. Geometrical and topological effects involving helicity, encountered

---

*Corresponding author. Email: jacobitz@sandiego.edu

in numerous turbulent flows with a wide spectrum of applications ranging from astro-, geo-, and plasma-physics to classical fluid- and aero-dynamics, can thus be characterized. For a review on helicity, we refer to Moffatt and Tsinober [5].

Helical structures, corresponding to swirling flow, are present in a variety of turbulent flows. In electrically conducting fluids, helical structures are responsible for the alpha effect which amplifies the magnetic field by the so-called dynamo action [6–8]. In the atmosphere, tornadoes and hurricanes are characterized by strong swirling motion. Helicity plots are used in meteorology to identify such strong storms and to forecast their genesis [9, 10]. Helicity is necessary to maintain strong localized atmospheric vortical structures [11]. Magnetic helicity plays a key role for the magnetic confinement of the plasma in thermonuclear fusion devices, such as tokamaks. Swirling motion, e.g., streamwise vortices in boundary layers, leading and trailing edge vortices shed from wings, can be frequently observed in aerodynamics [12].

Normalizing helicity by the norms of the corresponding vectors yields the relative helicity that corresponds to the cosine of the angle between both vectors. For the relative kinetic helicity, we thus have $h_u = H_u/(|\boldsymbol{u}||\boldsymbol{\omega}|)$. Helical structures are characterized by alignment or anti-alignment of velocity and vorticity vectors, which implies $h_u = \pm 1$. Prototypical examples for flows with maximal helicity are Beltrami flows, i.e., flows for which the velocity field is an eigenvector of the curl operator. Maximum helicity, the perfect alignment of velocity and vorticity, results in a local depletion of the nonlinear term in the Navier–Stokes equation [13, 14], which is known as local flow Beltramization. In this case, the Lamb vector, i.e., the vector product between velocity and vorticity vanishes, so that the whole nonlinear term, which corresponds to the solenoidal part of the Lamb vector, is locally equal to zero.

In Kerr [15], helicity and strain have been studied in forced isotropic turbulence considering histograms, while Pelz et al. [14] investigated local helicity in turbulent channel flow and turbulent Taylor–Green flow. Shell models of isotropic turbulence have been used to study helicity and its transfer [16, 17]. High-resolution direct numerical simulations of forced helical rotating turbulence have been studied in Mininni and Pouquet [18, 19]. The alignment of velocity and vorticity in various flow types, such as shear flow, channel flow, and strained flow, was examined in Rogers and Moin [20]. In their simulations, it was shown that the alignment of velocity and vorticity was significantly weaker than in the investigation of Pelz et al. [14]. They questioned the results of the latter and the role of helicity fluctuations in three-dimensional turbulence in general. The generation and destruction mechanisms of cross helicity, defined by the scalar product between the velocity and the magnetic field, in magnetohydrodynamic turbulence have been studied in Yokoi [21].

The balance equation for mean kinetic helicity has been discussed by Sanada [22] for isotropic turbulence. Sanada conjectured that the dissipation of mean kinetic helicity $\langle H_u \rangle$ is determined by mean super-helicity $\langle H_\omega \rangle = \langle \boldsymbol{\omega} \cdot (\nabla \times \boldsymbol{\omega}) \rangle$. Since the two mean helicities are signed quantities, mean super-helicity can dissipate mean kinetic helicity only if the two quantities have the same sign. Evidence supporting Sanada's conjecture was given more recently by Galanti and Tsinober [23] for isotropic turbulence with helical or non-helical forcing.

In Jacobitz et al. [24], the influence of initial mean kinetic helicity was studied for homogeneous turbulent shear flow. In order to gain insight into the evolution of the kinetic energy and kinetic helicity, an analysis of the spectral tensor, the two-point correlation of velocity in Fourier space, was performed (see also Cambon et al. [25] and Sagaut and Cambon [26]). The spectral tensor was decomposed into its mirror-symmetric part (related to kinetic energy) and its anti-symmetric part (related to kinetic helicity). This

analysis showed that the evolution equations of the two parts are only linked through the nonlinear interaction terms. Therefore, kinetic helicity only influences the evolution of kinetic energy through the nonlinear term. The influence of initial mean kinetic helicity on the flow evolution resembles the influence of mean kinetic helicity on decaying isotropic turbulence: the initial decay of the kinetic energy is weakened. This finding is in agreement with Kraichnan's prediction that energy transfer is slowed down by helical motion [27].

The helical properties of rotating sheared turbulence were investigated in Jacobitz et al. [28]. It was concluded that the growing cases are characterized by a tendency toward local two-dimensionalization, while decaying cases exhibit a preference for swirling motion. A motivation for the present study is to investigate if these findings hold for a wider class of homogeneous turbulent flows.

In the present study, the helical properties of six cases are investigated: a solenoidal uncorrelated Gaussian random field, statistically steady forced isotropic turbulence [29], decaying isotropic turbulence [30], decaying rotating turbulence [31], growing sheared turbulence, and growing rotating sheared turbulence with a rotation ratio $f/S = +0.5$ [28, 32]. The turbulent flows were studied using direct numerical simulations and details can be found in the respective publications. All cases initially do not contain mean kinetic helicity and they remain free from it. However, this does not concern the local kinetic helicity and regions with strong kinetic helicity can exist in a flow free from mean kinetic helicity.

The purpose of this study is to answer three questions: first, what are the local helical properties of the turbulent flows, and are the helical properties related to the fate, growth, or decay of the turbulence? Second, do helical properties vary with the scale of the turbulent motion? This question is addressed using a wavelet-based decomposition of the turbulent motion into different scales as proposed in Yoshimatsu et al. [33]. Third, does super-helicity act to diminish kinetic helicity?

2. Results

In this section, the helical properties of a solenoidal Gaussian random field, statistically steady forced isotropic turbulence, decaying isotropic turbulence, decaying rotating turbulence, growing sheared turbulence, and growing rotating sheared turbulence are presented first. Then, a wavelet-based scale-dependent analysis considers helicity at different scales of turbulent motion. Finally, the role of super-helicity as a dissipative mechanism for kinetic helicity is investigated.

An overview of the different flows is given in Table 1. The statistically steady forced isotropic turbulence case of Vincent and Meneguzzi [29] has a Taylor microscale Reynolds number $Re_\lambda = 150$. The decaying isotropic turbulence case of Jacobitz et al. [30] is taken at an eddy-overturning time $t^* = t\epsilon/K = 3$, where $K = \langle u_k u_k \rangle/2$ is the turbulent kinetic

Table 1. Properties of the turbulent flows considered in this study.

Case	Source	Re_λ	Fate
Gaussian white noise			
Forced isotropic turbulence	Vincent and Meneguzzi (1991)	150	Steady
Isotropic turbulence	Jacobitz et al. (2005)	27	Decay
Rotating turbulence	Liechtenstein et al. (2005)	60	Decay
Sheared turbulence	Jacobitz et al. (2008)	72	Growth
Rotating and sheared	Jacobitz et al. (2008)	100	Growth

energy, $\epsilon = \nu \langle \partial u_i / \partial x_k \partial u_i / \partial x_k \rangle$ is the dissipation rate, and ν is the kinematic viscosity. The Taylor microscale Reynolds number is $Re_\lambda = q\lambda/\nu = 27$, where $q = \sqrt{2K}$ is the magnitude of velocity and $\lambda = \sqrt{5\nu q^2/\epsilon}$ is the Taylor microscale. The decaying rotating turbulence by Liechtenstein et al. [31] is taken at an eddy-overturning time $t^* = 3$. The Taylor microscale Reynolds number is $Re_\lambda = 60$ and the Rossby number is $Ro = q/(fL) = 0.025$, where $f = 2\Omega$ is the Coriolis parameter and L is an integral length scale. The growing sheared turbulence and growing rotating sheared turbulence by Jacobitz et al. [32] are taken at a non-dimensional time $St = 5$, where S is the uniform mean shear. The Taylor microscale Reynolds numbers are $Re_\lambda = 72$ and $Re_\lambda = 100$, respectively. The shear numbers are $SK/\epsilon = 4.8$ and $SK/\epsilon = 6.0$, respectively. For the rotating sheared turbulence case, the rotation ratio is $f/S = +0.5$ and the Rossby number is $Ro = 0.166$. All flows were studied using direct numerical simulations based on a Fourier-pseudospectral method at a resolution of 256^3 grid points.

2.1. *Helical properties of the flows*

Figure 1 shows the probability distribution functions (PDFs; estimated from a histogram with 100 equidistant bins) of relative kinetic helicity h_u for the six cases considered in this study. For the case of the solenoidal Gaussian random field, a uniform distribution is obtained without a preference for any value of h_u. The two cases of statistically steady forced isotropic turbulence and decaying isotropic turbulence are characterized by maxima at $h_u = \pm 1$, corresponding to a higher probability for alignment or anti-alignment of velocity and vorticity, i.e., helical or swirling motion. The decaying rotating turbulence case shows an approximately even distribution of relative kinetic helicity with just a slight maximum at $h_u = +1$. The two cases of growing sheared turbulence and growing rotating sheared turbulence with $f/S = +0.5$, however, exhibit a maximum at $h_u = 0$, corresponding to a preference for velocity and vorticity to be perpendicular, i.e., local two-dimensionalization of the flows.
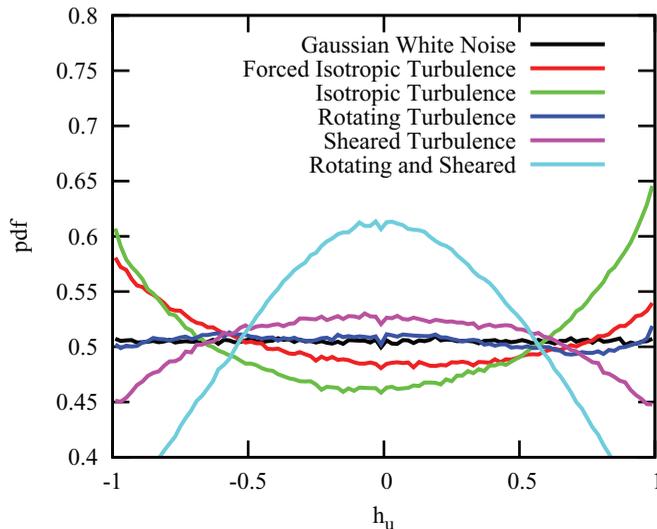
Figure 1.   PDFs of relative kinetic helicity h_u for the six cases.

It is found that growing turbulence has a tendency to local two-dimensionalization of the flow, while decaying turbulence is characterized by helical motion. Statistically steady forced isotropic turbulence shows a trend similar to the results obtained for decaying turbulence. These findings are consistent with a previous study restricted to rotating sheared turbulence with different rotation ratios [28]. Growing turbulence was observed for rotation ratios $0 \leq f/S \leq 1$, which corresponds to an anti-parallel arrangement of the system rotation and the flow's mean vorticity due to shear. For these growing cases, a preference for $h_u = 0$ was observed. For all other cases, including those with a parallel arrangement of system rotation and mean vorticity, decay of the turbulence was obtained. For those decaying cases, a preference of $h_u = \pm 1$ was found in the simulations. The local two-dimensionalization observed in the cases in which the kinetic energy is growing is to a certain extent consistent with the fact that in two-dimensional flows the energy is less efficiently transferred to the small scales than in three-dimensional flows. For shear flows, these finding are consistent with a higher likelihood of vanishing kinetic helicity in regions of low-energy dissipation rate [34]. The interpretation of the helical motion for the remaining flows is not entirely clear. The local helical properties observed in the decaying or statistically steady flows indicate clearly the three-dimensional character of these flows, and in the isotropic case this is consistent with an energy cascade toward small scales, which is more efficient than for two-dimensional turbulence. However, these local helicity fluctuations do at the same time weaken the nonlinear term, so that the transfer of energy to small scales is not optimal.

The corresponding PDFs of relative super-helicity h_ω are given in Figure 2. Again, for the solenoidal Gaussian random field, a uniform distribution is obtained without a preference for any value of h_ω. In contrast to the relative kinetic helicity h_u, the relative super-helicity h_ω shows pronounced maxima at $h_\omega = \pm 1$ for all turbulent flows and it does not aid with a further classification of the fate of the flows. This result is again in agreement with the previous study of rotating sheared turbulence by Jacobitz et al. [28].
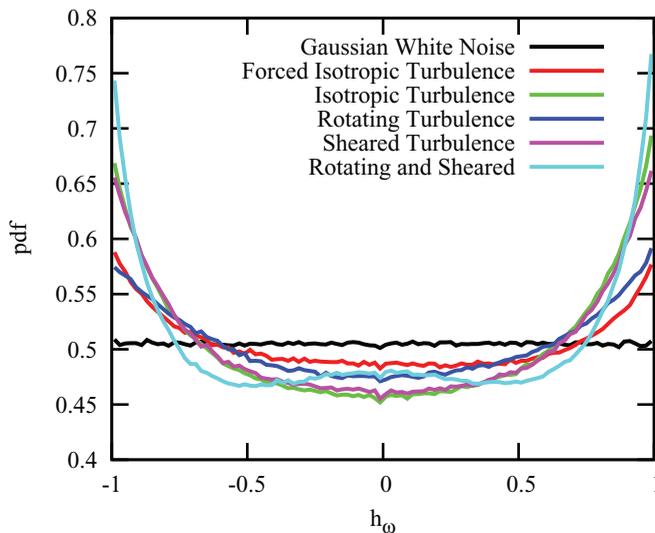
Figure 2.   PDFs of relative super-helicity h_ω for the six cases.

2.2. *Scale-dependent analysis*

The wavelet representation of turbulent flows (see, for example, Farge [35] as well as Schneider and Vasilyev [36]) allows for a clear scale separation. To obtain the scale contributions of velocity $\mathbf{u}^j$ (and similarly for vorticity and its curl), the flow field $\mathbf{u} = (u_1, u_2, u_3)$, given at resolution $N = 2^{3J}$ with $J = 8$, is decomposed into an orthogonal wavelet series using Coiflet 12 wavelets:

$$\mathbf{u}(\mathbf{x}) = \sum_{\lambda} \widetilde{\mathbf{u}}_{\lambda} \psi_{\lambda}(\mathbf{x}). \tag{1}$$

The multiindex $\lambda = (j, \mathbf{i}, \mu)$ denotes scale index j (with $0 \leq j \leq J - 1$), spatial position $\mathbf{i}$ (with 2^{3j} values for each j and μ), and seven spatial directions $\mu = 1, \ldots, 7$ of each wavelet ψ_{λ} [35]. Due to the orthogonality of the wavelets, the coefficients are given by $\widetilde{\mathbf{u}}_{\lambda} = \langle \mathbf{u}, \psi_{\lambda} \rangle$, where $\langle \cdot, \cdot \rangle$ denotes the L^2-inner product. The coefficients measure fluctuations of $\mathbf{u}$ at scale 2^{-j} and around position $\mathbf{i}/2^j$ for each of the seven possible directions. Fixing j and summing only over $\mathbf{i}$ and μ in Equation (1), the contribution $\mathbf{u}^j$ at scale j is obtained and by construction we have $\mathbf{u} = \sum_j \mathbf{u}^j$. Analogously, the contributions ω^j and $(\nabla \times \omega)^j$ at scale 2^{-j} are obtained.

Thus, the scale-dependent kinetic helicity can be defined as follows:

$$H_{u^j} = \mathbf{u}^j \cdot \boldsymbol{\omega}^j. \tag{2}$$

Here, $\mathbf{u}^j$ and $\boldsymbol{\omega}^j$ are velocity and vorticity at scale 2^{-j}, respectively, as proposed in Yoshimatsu et al. [33] for isotropic turbulence. For $j \neq 0$, the scale-dependent kinetic helicity H_{u^j} is a Galilean invariant of the flow, though H_u itself is not. This is based on the fact that the mean velocity of $\mathbf{u}^j$ vanishes due to the vanishing moment property of the wavelets [35].

Accordingly, the scale-dependent relative kinetic helicity can be defined as

$$h_{u^j} = H_{u^j}/(|\boldsymbol{u}^j||\boldsymbol{\omega}^j|). \tag{3}$$

Analogously, the scale-dependent super-helicity $H_{\omega^j} = \boldsymbol{\omega}^j \cdot (\nabla \times \boldsymbol{\omega})^j$ and the corresponding relative quantity h_{ω^j} are obtained. These scale-dependent quantities yield further insight into the geometrical statistics at different scales of motion. In the following, we analyze the different turbulent flows.

PDFs of scale-dependent relative kinetic helicity h_{u^j} (left column) and relative super-helicity h_{ω^j} (right column) are presented in Figures 3 and 4 for the six different cases considered here. The figures show the PDFs of the total relative helicities and the PDFs of the scale-dependent helicities at scales $j = 3$ to $j = 7$. Note that largest scales $j = 1$ and $j = 2$ are not shown, since the flow contains only a small number of wavelet modes at those scales and the PDFs are consequently poorly converged.

For the solenoidal Gaussian random field (3, top), the uniform distribution for the total helicities persists at all scales as expected. For statistically steady forced isotropic turbulence (3, center), decaying isotropic turbulence (3, bottom), and decaying rotating turbulence (4, top), the smallest scales of motion show maxima at $h_{u^j} = \pm 1$. In the case of forced isotropic turbulence, the maxima at $h_{u^j} = \pm 1$ for smaller scales are the least pronounced, but a maximum at $h_{u^j} = 0$ is observed for the larger scales. For decaying isotropic turbulence and decaying rotating turbulence, the larger scales of motion do not
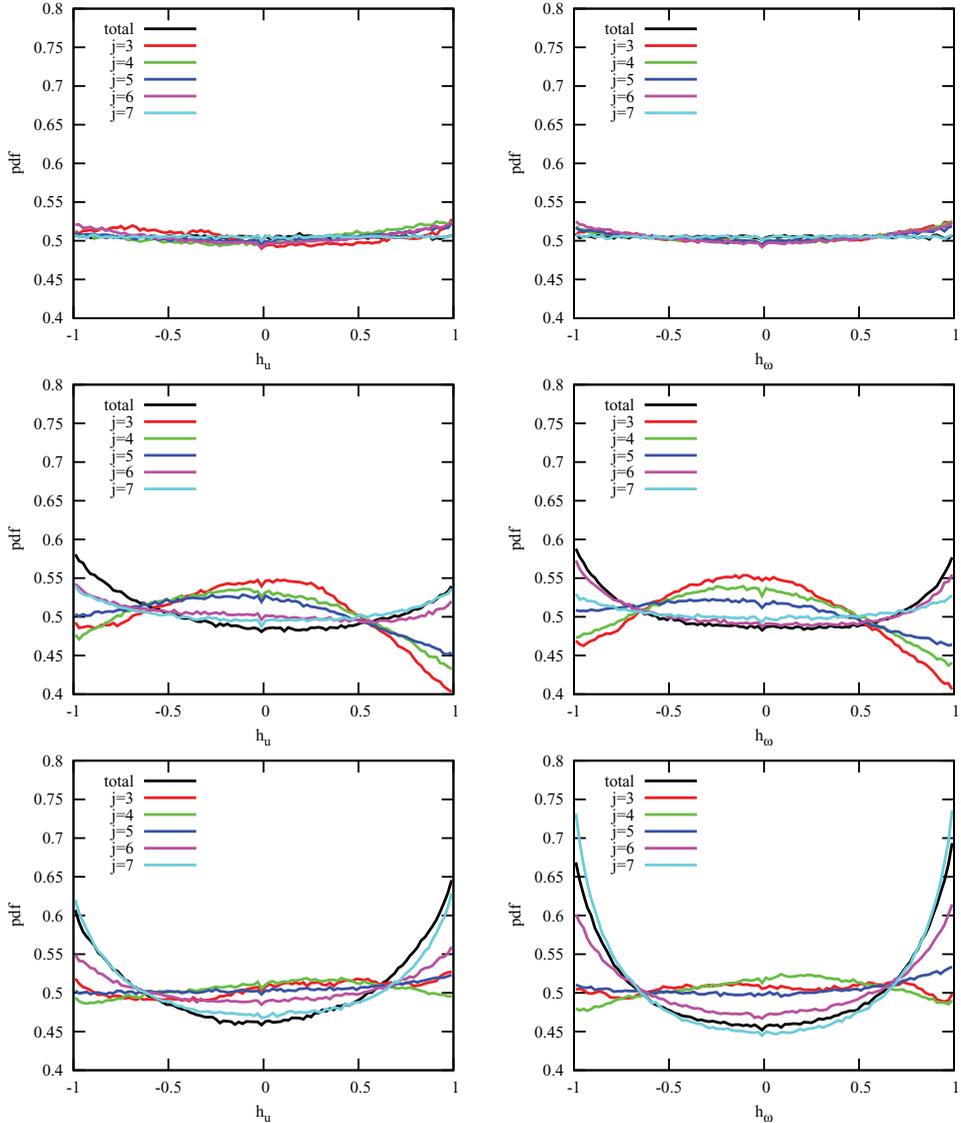
Figure 3. PDFs of scale-dependent kinetic helicity h_{u^j} (left column) and super-helicity h_{ω^j} (right column) for a Gaussian random field (top), forced isotropic turbulence (center), and decaying isotropic turbulence (bottom).

show a clearly defined maximum. For growing sheared turbulence (4, center), the PDFs of scale-dependent relative kinetic helicity of the larger scales with $j = 3, 4$, and 5 show a maximum at $h_{u^j} = 0$, corresponding to a trend to local two-dimensionalization of the flow at large scales. The smaller scales with $j = 6$ and 7 have maxima at $h_{u^j} = \pm 1$, corresponding to a trend to helical motion at small scales. For growing rotating sheared turbulence with $f/S = +0.5$ (4, bottom), a similar result as for sheared turbulence is obtained, but the probability for local two-dimensionalization at large scales and helical motion at small scales is even more pronounced.
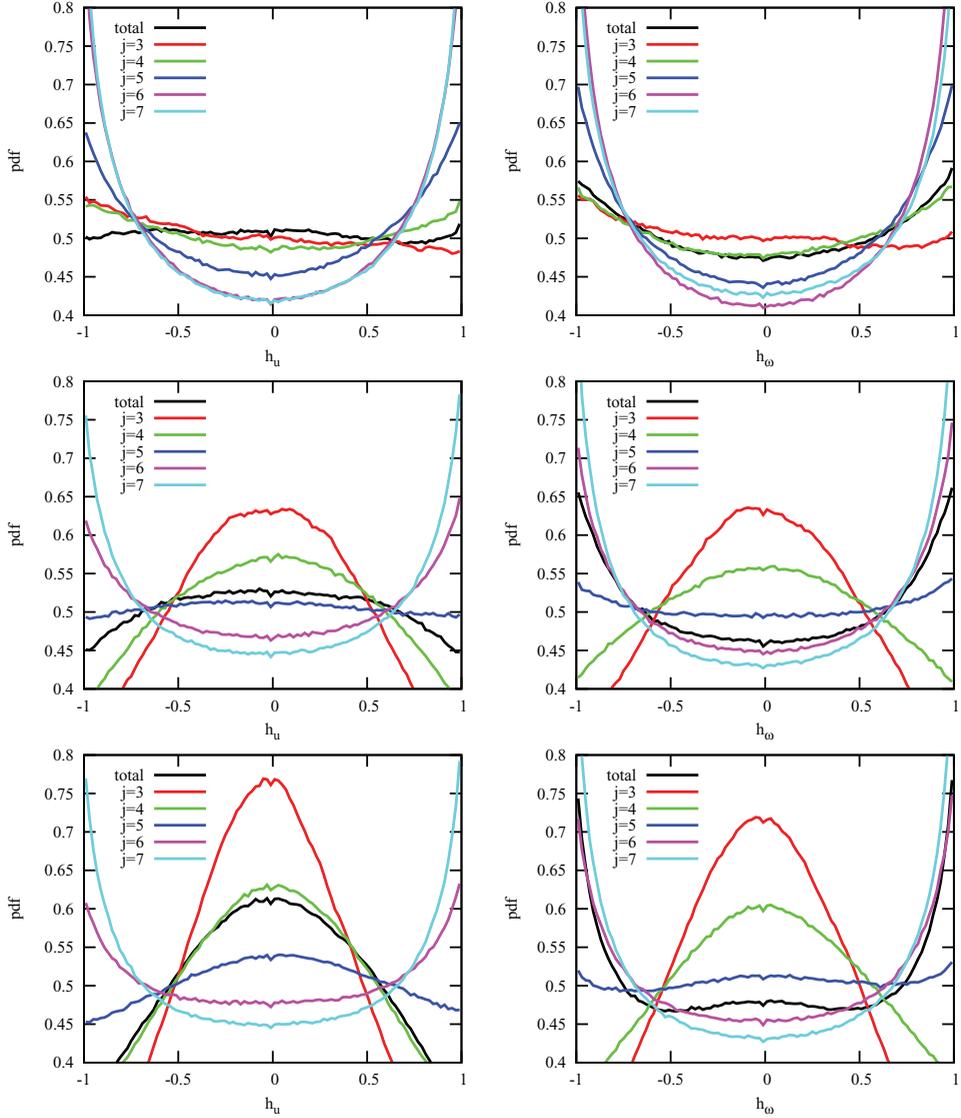
Figure 4. PDFs of scale-dependent kinetic helicity h_{u^j} (left column) and super-helicity h_{ω^j} (right column) for decaying rotating turbulence (top), growing sheared turbulence (center), and growing rotating sheared turbulence with $f/S = +0.5$ (bottom).

The PDFs of scale-dependent relative super-helicity of these three cases also yield a maximum at $h_{\omega^j} = 0$ for the larger scales with $j = 3, 4$, and 5 and maxima at $h_{\omega^j} = \pm 1$ at the smaller scales $j = 6$ and 7. For decaying rotating turbulence and decaying rotating sheared turbulence with $f/S = +5$, the scale-dependent kinetic helicity PDFs show maxima for $h_{u^j} = \pm 1$ at all scales $j > 3$. Similarly, the scale-dependent relative super-helicity PDFs yield maxima for $h_{\omega^j} = \pm 1$ for all scales considered.

The decomposition of velocity and vorticity into scale-dependent contributions first as well as the decomposition of the kinetic helicity directly yield the same mean kinetic

helicity values for each scale 2^{-j}, i.e., the sum over j of the scalewise mean helicities results in the total mean helicity. This property is similar to the feature obtained for the helicity spectrum, i.e., the sum of the helicity spectrum over all wavenumbers yields the total mean helicity. The reason for the equivalence of both decompositions is that the wavelets are orthogonal with respect to scale index j. Thus, the velocity components u^j and the vorticity components ω^j are orthogonal, i.e., $\langle u^j, \omega^{j'} \rangle = 0$ for $j \neq j'$. However, the pointwise scale-dependent helicities differ.

In analogy to the spectrum, we prefer to use the scale decomposition of velocity and vorticity. This scale-dependent helicity could be called helicity scalogram (contributions of helicity per scale) in analogy with the energy scalogram (contribution of energy per scale), where the velocity is decomposed in scale contributions and not the energy. The scalograms can be related to Fourier spectra, using a relation between the scale index j and the wavenumber $k_j = k_\psi 2^j$, where k_ψ is the centroid wavenumber of the wavelet [35]. The scalogram corresponds to a smoothed version of the Fourier spectrum. The smoothing kernel is the square of the Fourier transform of the wavelet. As frequency increases, i.e., at small scales, the smoothing interval becomes larger, which explains why the wavelet spectrum is a well-conditioned statistical estimator.

The scale-dependent helicity introduced in Rodriguez Imazio and Mininni [37] corresponds to a low-pass-filtered helicity, considering decreasing box sizes, whereas the wavelet-based scale-dependent helicity corresponds to a band-pass-filtered helicity, considering bands of increasing wavenumber, which yields incremental information on the helicity of the flow scale by scale. The latter quantity can be compared with the Fourier helicity spectrum, which gives the helicity distribution wavenumber by wavenumber, whereas the former gives some cumulative information, since information on the helicity of the larger scale contributions of the flow is included in the helicity of the smaller scale contributions. Hence, both quantities do not yield the same values.

2.3. *Dissipation of kinetic helicity*

The evolution of mean kinetic helicity $\langle H_u \rangle$ is described by a transport equation:

$$\frac{d}{dt} \langle H_u \rangle = -2\nu \langle H_\omega \rangle + \langle F \rangle. \tag{4}$$

Here, $F = 2\boldsymbol{f} \cdot \boldsymbol{\omega}$ accounts for the forcing term $\boldsymbol{f}$ in the momentum equation and vanishes for the flows considered here due to their mirror symmetry property. The kinematic viscosity of the fluid is ν. Dissipation of mean kinetic helicity $\langle H_u \rangle$ by mean super-helicity $\langle H_\omega \rangle$ requires that both mean helicities have the same sign. Sanada [22] conjectured that the two helicities indeed have the same sign for isotropic turbulence.

Motivated by this study, further evidence to support a local dissipative mechanism of kinetic helicity by super-helicity is provided: first, the PDFs of the cosine of the angle between velocity and the curl of vorticity are considered. Second, the joint PDFs of relative kinetic helicity with relative super-helicity are determined. Third, the two relative helicities are used to color isosurfaces of vortical structures.

Using the vector identity

$$\nabla \times \nabla \times \boldsymbol{u} = -\nabla^2 \boldsymbol{u}, \tag{5}$$

it follows that

$$\boldsymbol{u} \cdot \nabla \times \nabla \times \boldsymbol{u} = \boldsymbol{\omega} \cdot \boldsymbol{\omega} - \nabla \cdot (\boldsymbol{u} \times \boldsymbol{\omega}). \tag{6}$$

Averaging over a domain with periodic boundary conditions or boundaries on which the normal component of $\boldsymbol{u} \times \boldsymbol{\omega}$ vanishes leads then to the expression

$$\langle \boldsymbol{u} \cdot \nabla \times \nabla \times \boldsymbol{u} \rangle = \langle \boldsymbol{\omega} \cdot \boldsymbol{\omega} \rangle > 0. \tag{7}$$

It can, therefore, be deduced that there is a larger probability that the vectors $\boldsymbol{u}$ and $\nabla \times \nabla \times \boldsymbol{u}$ are aligned than that they are anti-aligned. From the larger probability of alignment, it follows that there is a larger likelihood that the kinetic helicity $H_u = \boldsymbol{u} \cdot \boldsymbol{\omega}$ and the super-helicity $H_\omega = \boldsymbol{\omega} \cdot \nabla \times \boldsymbol{\omega}$ have the same sign [22]. The higher likelihood for the same sign also applies to the relative helicities h_u and h_ω [23].

Figure 5 shows the PDF of the cosine of the angle between velocity $\boldsymbol{u}$ and the curl of vorticity $\nabla \times \nabla \times \boldsymbol{u} = -\nabla^2 \boldsymbol{u}$ for the six cases. The PDFs are strongly skewed supporting a high probability for the alignment of the two vectors. The most strongly skewed PDF is observed for the solenoidal Gaussian random field, indicating that the alignment is a kinematic property of the curl operator. In contrast, the least skewed PDF is found for forced isotropic turbulence. For the four remaining cases, all directly computed from the Navier–Stokes equations, the PDFs are similar with maxima in between those found for the random field and the forced isotropic turbulence case.

The impact of forcing in isotropic turbulence simulations on the alignment is investigated in more detail in Figure 6. The figure shows decaying isotropic turbulence and results from three well-developed forced isotropic turbulence simulations by Vincent and Meneguzzi [29], Yeung et al. [38], and da Silva et al. [39]. The three forced isotropic turbulence fields are chosen at a time corresponding to the statistically steady regime. Different forcing methods are used in these studies: Vincent and Meneguzzi [29] use a deterministic
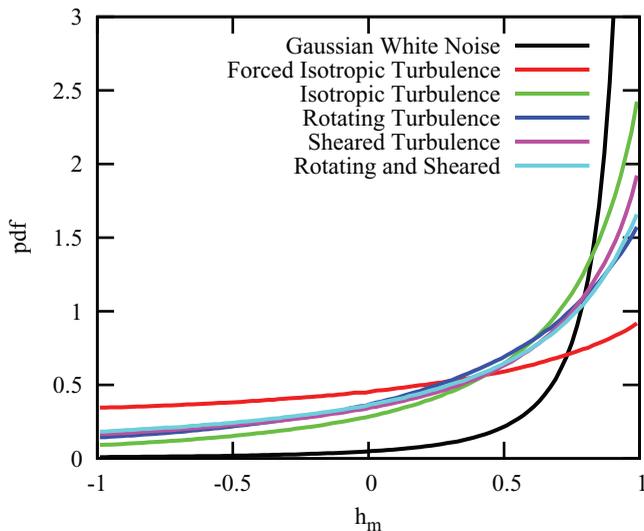
Figure 5. PDFs of the cosine of the angle between velocity u and curl of vorticity $\nabla \times \nabla \times u$ for the six cases.
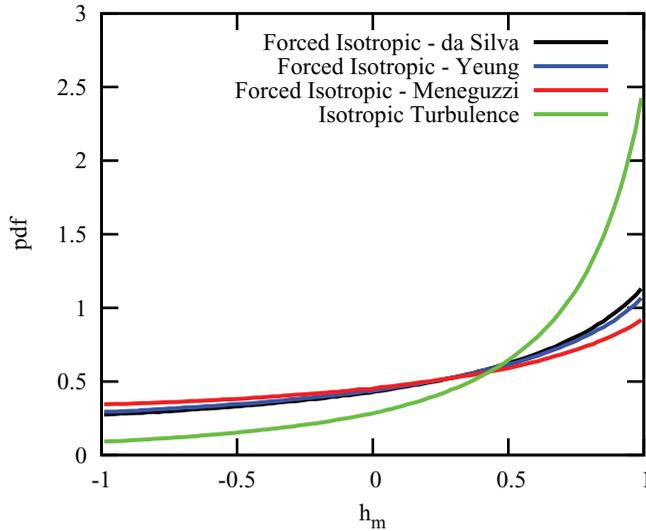
Figure 6. PDFs of the cosine of the angle between velocity u and curl of vorticity $\nabla \times \nabla \times u$ for isotropic turbulence cases.

forcing mechanism with a constant amplitude for all Fourier modes with wavenumber components equal to zero or one as described by Kerr [40]. Yeung et al. [38] use the stochastic forcing scheme by Eswaran and Pope [41]. The forcing consists of a forcing acceleration in the low wavenumber band, which is based on an Ornstein-Uhlenbeck random process (six in total). The work of da Silva et al. [39] uses the stochastic volume forcing algorithm developed by Alvelius [42]. The results suggest that the forcing mechanisms employed in the forced isotropic turbulence simulations have an impact on the alignment of velocity and the curl of vorticity. It appears that the forcing mechanisms also introduce a small amount of mean kinetic helicity and the resulting PDF of relative kinetic helicity is not symmetric around zero (see Figure 1).

To further verify that there is a high probability that the two helicities even locally have the same sign, joint PDFs of relative kinetic helicity h_u with relative super-helicity h_ω are shown in Figure 7. For all cases, a strong correlation of the signs of the two helicities is indeed observed. This sign correlation thus supports that super-helicity diminishes kinetic helicity.

Note that the one-dimensional PDFs of h_u and h_ω can be obtained by integration of the joint PDF over h_ω and h_u, respectively. Therefore, a joint PDF that is approximately symmetric along its diagonal axis will yield similarly shaped PDFs for h_u and h_ω. These features are indeed observed for cases with decaying turbulent kinetic energy, forced isotropic turbulence, and the Gaussian random field. In contrast, one possibility to obtain different shapes for the PDFs of h_u and h_ω is an asymmetric joint PDF. Hence, this symmetry is broken for the cases with growing turbulent kinetic energy.

Figure 8 shows isovorticity surfaces for three of the six cases considered here: forced isotropic turbulence (top), decaying rotating turbulence (center), and growing sheared turbulence (bottom). No preferred orientation is visible in the case of forced isotropic turbulence. Vertical columns are present in rotating turbulence, while inclined structures are observed for sheared turbulence. The isovorticity surfaces are colored with relative
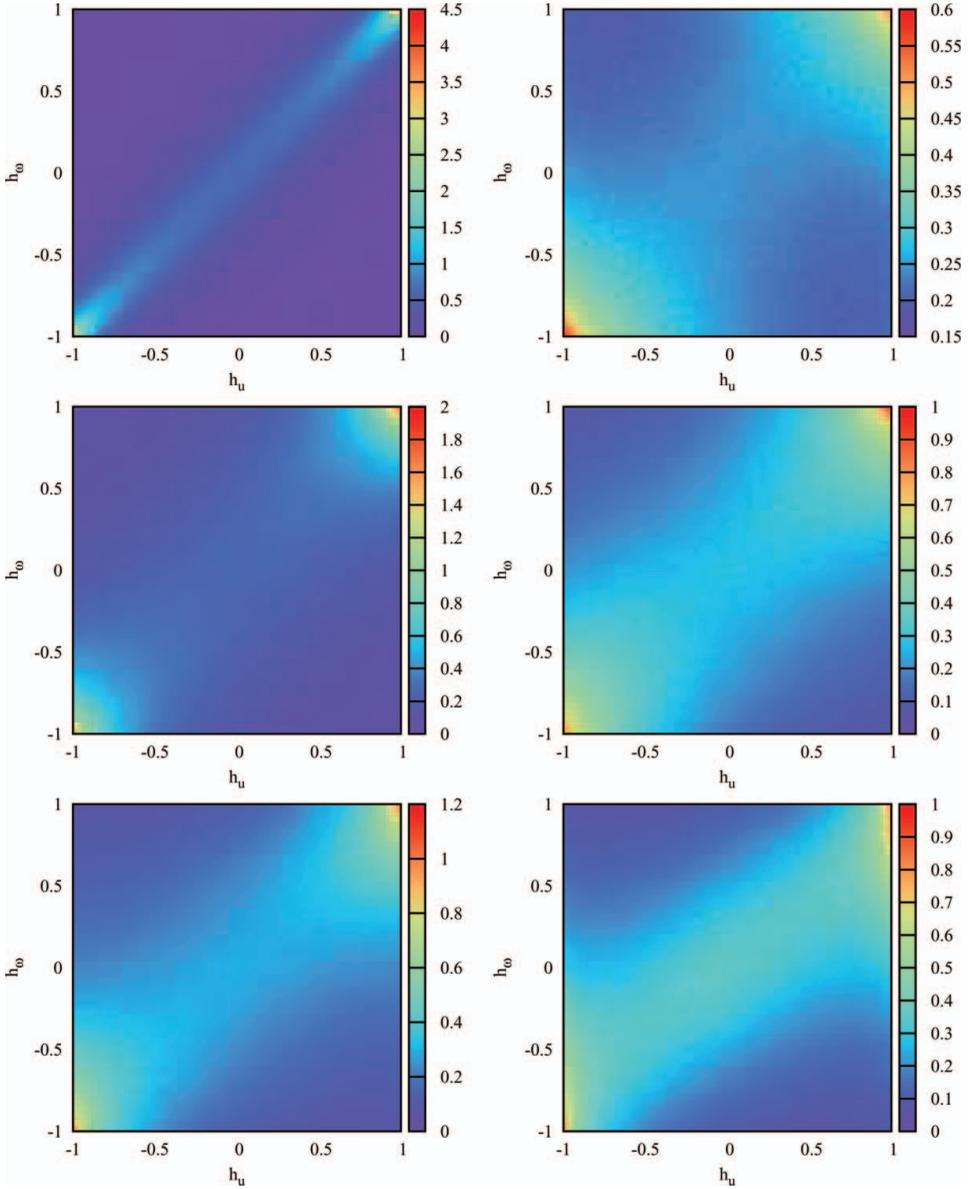
Figure 7. Joint PDFs of kinetic helicity h_u and super-helicity h_ω for a Gaussian random field (top left), forced isotropic turbulence (top right), decaying isotropic turbulence (center left), rotating turbulence (center right), sheared turbulence (bottom left), and growing rotating sheared turbulence with $f/S = +0.5$ (bottom right).

kinetic helicity h_u (left) and relative super-helicity h_ω (right). For a given flow structure, it is likely that the same sign is found. This visual observation thus indicates a high likelihood that the signs of h_u and h_ω are indeed correlated.

All indicators considered in this study suggest that super-helicity acts as a dissipative process for kinetic helicity also locally in anisotropic homogeneous turbulence.
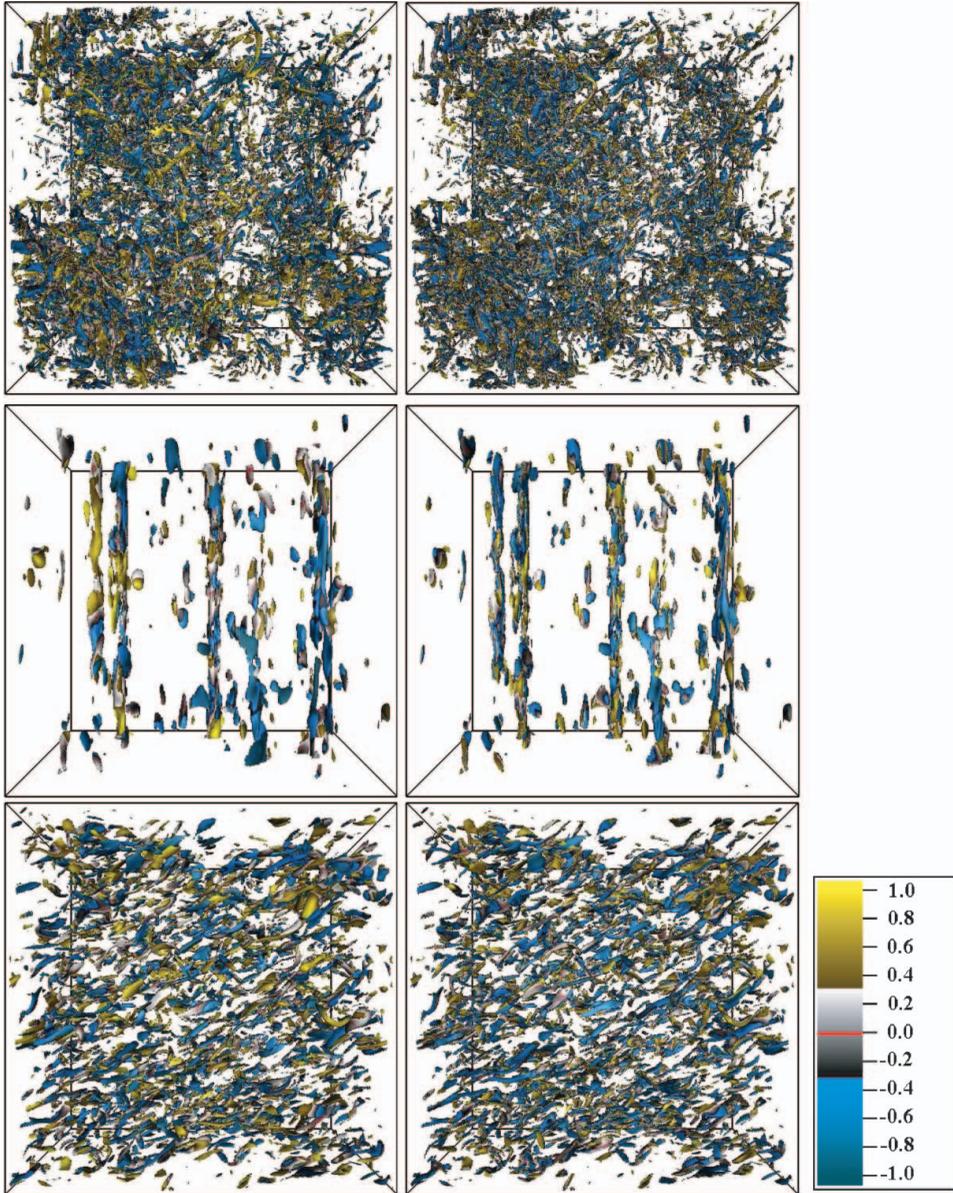
Figure 8. Isovorticity structures colored with kinetic helicity h_u (left) and super-helicity h_ω (right) for forced isotropic turbulence (top), rotating turbulence (center), and sheared turbulence (bottom).

3. Conclusions

To summarize, helical properties of five prototypical turbulent flows were investigated and compared to the helical properties of a solenoidal Gaussian random field. For the PDFs of kinetic helicity h_u, a maximum at $h_u = 0$ was observed for cases with growing turbulent kinetic energy, while a maximum at $h_u = \pm 1$ was found for decaying cases. Thus, for growing cases, the PDFs of kinetic helicity h_u indicate a larger probability that

velocity and vorticity are perpendicular, corresponding to local two-dimensionalization of the flow. This finding is consistent with the two-dimensionalization of the fluctuating strain rate for growing turbulent shear flow [43]. For decaying cases, the PDFs of kinetic helicity h_u show a preference for the alignment or anti-alignment of velocity and vorticity, corresponding to helical motion. For all cases, however, the PDFs of super-helicity h_ω always assume a maximum at $h_\omega = \pm 1$. The helical properties of the statistically steady forced isotropic turbulence case were found to follow those of flows with decaying turbulent kinetic energy.

Scale-dependent PDFs of kinetic helicity show that large scales tend to have a maximum at $h_{u^j} = 0$, corresponding to two-dimensionalization of the flows, while small scales tend to show a maximum at $h_{u^j} = \pm 1$, corresponding to helical motion. These observations hold for all types of turbulent flows considered in this study.

Consideration of the alignment of velocity with the curl of vorticity, joint PDFs of relative kinetic helicity and relative super-helicity, as well as isovorticity surfaces colored with kinetic helicity and super-helicity all indicate a high probability that h_u and h_ω have the same sign even locally. Thus, super-helicity tends to diminish kinetic helicity for the different homogeneous turbulent flows studied here.

References

[1] R. Betchov, *Semi-isotropic turbulence and helicoidal flows*, Phys. Fluids 4 (1961), pp. 925–926.
[2] M.A. Berger and G.B. Field, *The topological properties of magnetic helicity*, J. Fluid Mech. 147 (1984), pp. 133–148.
[3] H.K. Moffatt, *The degree of knottedness of tangled vortex lines*, J. Fluid Mech. 35 (1969), pp. 117–129.
[4] J.-J. Moreau, *Constants d'un ilôt tourbillonnaire en fluide parfait barotrope*, C. R. Acad. Sci., Paris 252 (1961), pp. 2810–2812.
[5] H.K. Moffatt and A. Tsinober, *Helicity in laminar and turbulent flow*, Annu. Rev. Fluid Mech. 24 (1992), pp. 281–312.
[6] E.N. Parker, *Hydromagnetic dynamo models*, Astrophys. J. 122 (1955), pp. 293–314.
[7] A. Pouquet, M. Lesieur, and J. Leorat, *Strong MHD helical turbulence and the non-linear dynamo effect*, J. Fluid Mech. 77 (1976), pp. 321–354.
[8] M. Steenbeck, F. Kause, and K.H. Rädler, *Berechnung der mittleren Lorentz-Feldstärke für ein elektrisch leitendes Medium in turbulenter, durch Coriolis-Kräfte beeinflußter Bewegung*, Zs. f. Naturforschung 21a (1966), p. 369.
[9] G.V. Levina and M.T. Montgomery, *A first examination of the helical nature of tropical cyclogenesis*, Dokl. Earth Sci. 434 (2010), pp. 1285–1289.
[10] P.M. Markowski, J.M. Straka, E.N. Rasmussen, and D.O. Blanchard, *Variability of storm-relative helicity during VORTEX*, Mon. Weather Rev. 126 (1998), pp. 2959–2971.
[11] K.K. Droegemeier, S.M. Lazarus, and R. Davies-Jones, *The influence of helicity on numerically simulated convective storms*, Mon. Weather Rev. 21 (1993), pp. 2005–2029.

[12] M. Kholmyansky, M. Shapiro-Orot, and A. Tsinober, *Experimental observations of spontaneous breaking of reflectional symmetry in turbulent flow*, Proc. R. Soc. Lond. A 457 (2001), pp. 2699–2717.

[13] E. Levich and A. Tsinober, *On the role of helical structures in three-dimensional turbulent flow*, Phys. Lett. A 93 (1983), pp. 293–297.

[14] R. Pelz, V. Yakhot, S. Orszag, L. Shtilman, and E. Levich, *Velocity-vorticity patterns in turbulent flow*, Phys. Rev. Lett. 54 (1985), pp. 2505–2508.

[15] R.M. Kerr, *Histograms of helicity and strain in numerical turbulence*, Phys. Rev. Lett. 59 (1987), pp. 783–786.

[16] R. Benzi, L. Biferale, R. Kerr, and E. Trovatore, *Helical-shell models for three dimensional turbulence*, Phys. Rev. E 53 (1996), 3541.

[17] L. Biferale, D. Pierotti, and F. Toschi, *Helicity transfer in turbulent models*, Phys. Rev. E Rap. Comm. 57 (1998), R2515.

[18] P.D. Mininni and A. Pouquet, *Rotating helical turbulence. Part I. Global evolution and spectral behavior*, Phys. Fluids 22 (2010a), 035105.

[19] P.D. Mininni and A. Pouquet, *Rotating helical turbulence. Part II. Intermittency, scale invariance, and structures*, Phys. Fluids 22 (2010b), 035106.

[20] M.M. Rogers and P. Moin, *The structure of the vorticity field in homogeneous turbulent flows*, J. Fluid Mech. 176 (1987), pp. 33–66.

[21] N. Yokoi, *Modeling the turbulent cross-helicity evolution: production, dissipation, and transport rates*, J. Turbul. 12 (2011), N27.

[22] T. Sanada, *Helicity production in the transition to chaotic flow simulated by Navier-Stokes equation*, Phys. Rev. Lett. 70 (1993), pp. 3035–3038.

[23] B. Galanti and A. Tsinober, *Physical space properties of helicity in quasi-homogeneous forced turbulence*, Phys. Lett. A 352 (2006), pp. 141–149.

[24] F.G. Jacobitz, K. Schneider, W.J.T. Bos, and M. Farge, *Influence of initial mean helicity in homogeneous turbulent shear flow*, Phys. Rev. E 84 (2011), 056319.

[25] C. Cambon, D. Jeandel, and J. Mathieu, *Spectral modelling of homogeneous non-isotropic turbulence*, J. Fluid Mech. 104 (1981), pp. 247–262.

[26] P. Sagaut and C. Cambon, *Homogeneous Turbulence Dynamics*, Cambridge University Press, Cambridge, 2008.

[27] R.H. Kraichnan, *Helical turbulence and absolute equilibrium*, J. Fluid Mech. 59 (1973), pp. 745–752.

[28] F.G. Jacobitz, K. Schneider, W.J.T. Bos, and M. Farge, *On the structure and dynamics of sheared and rotating turbulence: Anisotropy properties and geometrical scale-dependent statistics*, Phys. Fluids 22 (2010), 085101.

[29] A. Vincent and M. Meneguzzi, *The spatial structure and statistical properties of homogeneous turbulence*, J. Fluid Mech. 225 (1991), pp. 1–20.

[30] F.G. Jacobitz, M.M. Rogers, and J.H. Ferziger, *Waves in stably stratified turbulent flow*, J. Turbul. 6 (2005), N32.

[31] L. Liechtenstein, F.S. Godeferd, and C. Cambon, *Nonlinear formation of structures in rotating stratified turbulence*, J. Turbul. 4 (2005), N24.

[32] F.G. Jacobitz, L. Liechtenstein, K. Schneider, and M. Farge, *On the structure and dynamics of sheared and rotating turbulence: Direct numerical simulation and wavelet-based coherent vortex extraction*, Phys. Fluids 20 (2008), 045103.

[33] K. Yoshimatsu, N. Okamoto, K. Schneider, Y. Kaneda, and M. Farge, *Intermittency and scale-dependent statistics in fully developed turbulence*, Phys. Rev. E 79 (2009), 026303.

[34] J.M. Wallace, *Twenty years of experimental and direct numerical simulation access to the velocity gradient tensor: What have we learned about turbulence?* Phys. Fluids 21 (2009), 021301.

[35] M. Farge, *Wavelet transforms and their applications to turbulence*, Annu. Rev. Fluid Mech. 24 (1992), pp. 395–458.

[36] K. Schneider and O.V. Vasilyev, *Wavelet methods in computational fluid dynamics*, Annu. Rev. Fluid Mech. 42 (2010), pp. 473–503.

[37] P. Rodriguez Imazio and P.D. Mininni, *Cancellation exponents in helical and non-helical flows*, J. Fluid Mech. 651 (2010), pp. 241–250.

[38] P.K. Yeung, D.A. Donzis, and K.R. Sreenivasan, *High-Reynolds-number simulation of turbulent mixing*, Phys. Fluids 17 (2005), 081703.

[39] C.B. da Silva, R.J.N. dos Reis, and J.C.F. Pereira, *The intense vorticity structures near the turbulent/non-turbulent interface in a jet*, J. Fluid Mech. 685 (2011), pp. 165–190.

[40] R. Kerr, *Higher-order derivative correlations and the alignment of small-scale structures in isotropic numerical turbulence*, J. Fluid Mech. 153 (1985), pp. 31–58.

[41] V. Eswaran and S.B. Pope, *An examination of forcing in direct numerical simulations of turbulence*, Comput. Fluids 16 (1988), pp. 257–278.

[42] K. Alvelius, *Random forcing of three-dimensional homogeneous turbulence*, Phys. Fluids 11 (1999), 1880.

[43] J.G. Brasseur and W. Lin, *Kinematics and dynamics of small-scale vorticity and strain-rate structures in the transition from isotropic to shear turbulence*, Fluid Dyn. Res. 36 (2005), pp. 357–384.